Electronic Supplementary Material (ESI) for Nanoscale.
This journal is © The Royal Society of Chemistry 2014

Porous carbon nitride nanosheets for enhanced photocatalytic activities

Jindui Hong,[ab] Shengming Yin,[ab] Yunxiang Pan,[a] Jianyu Han,[ab] Tianhua Zhou[ab] and Rong Xu*[ab]

[a] *School of Chemical & Biomedical Engineering, Nanyang Technological University, 62 Nanyang Drive, Singapore 637459. Fax: 65-67947553; Tel: 65-67906713; E-mail: rxu@ntu.edu.sg*

[b] *SinBeRISE CREATE, National Research Foundation, CREATE Tower level 11, 1 Create Way, Singapore 138602*

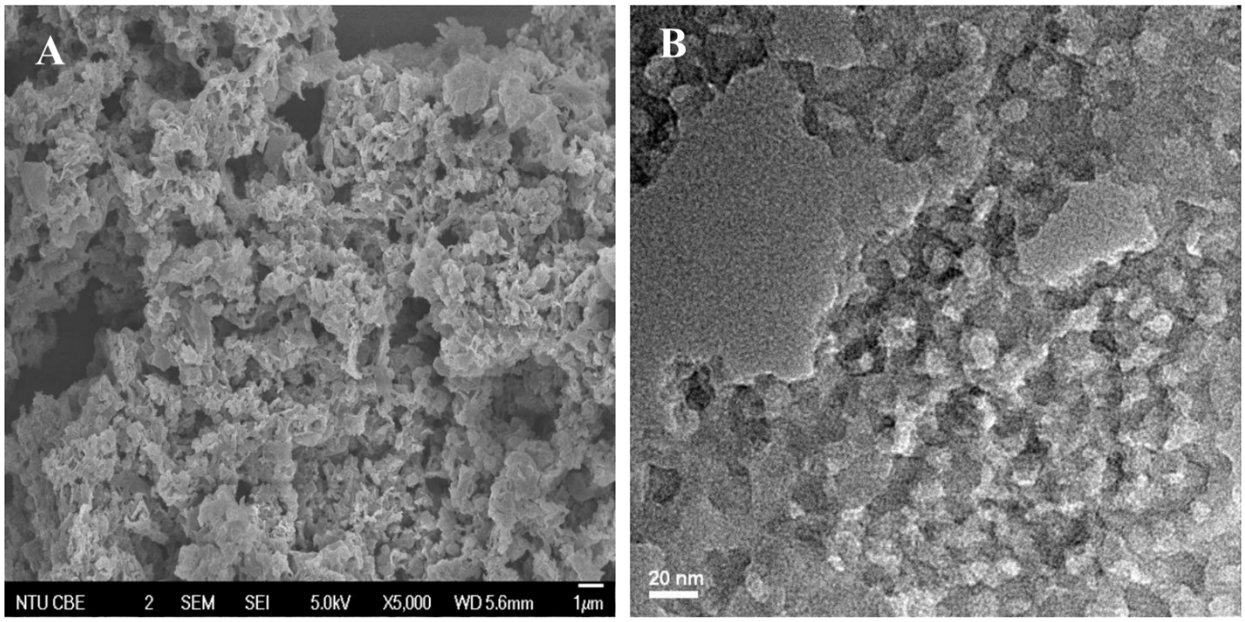

Figure S1. SEM (A) and TEM (B) images of porous carbon nitride (PCN) before exfoliation.

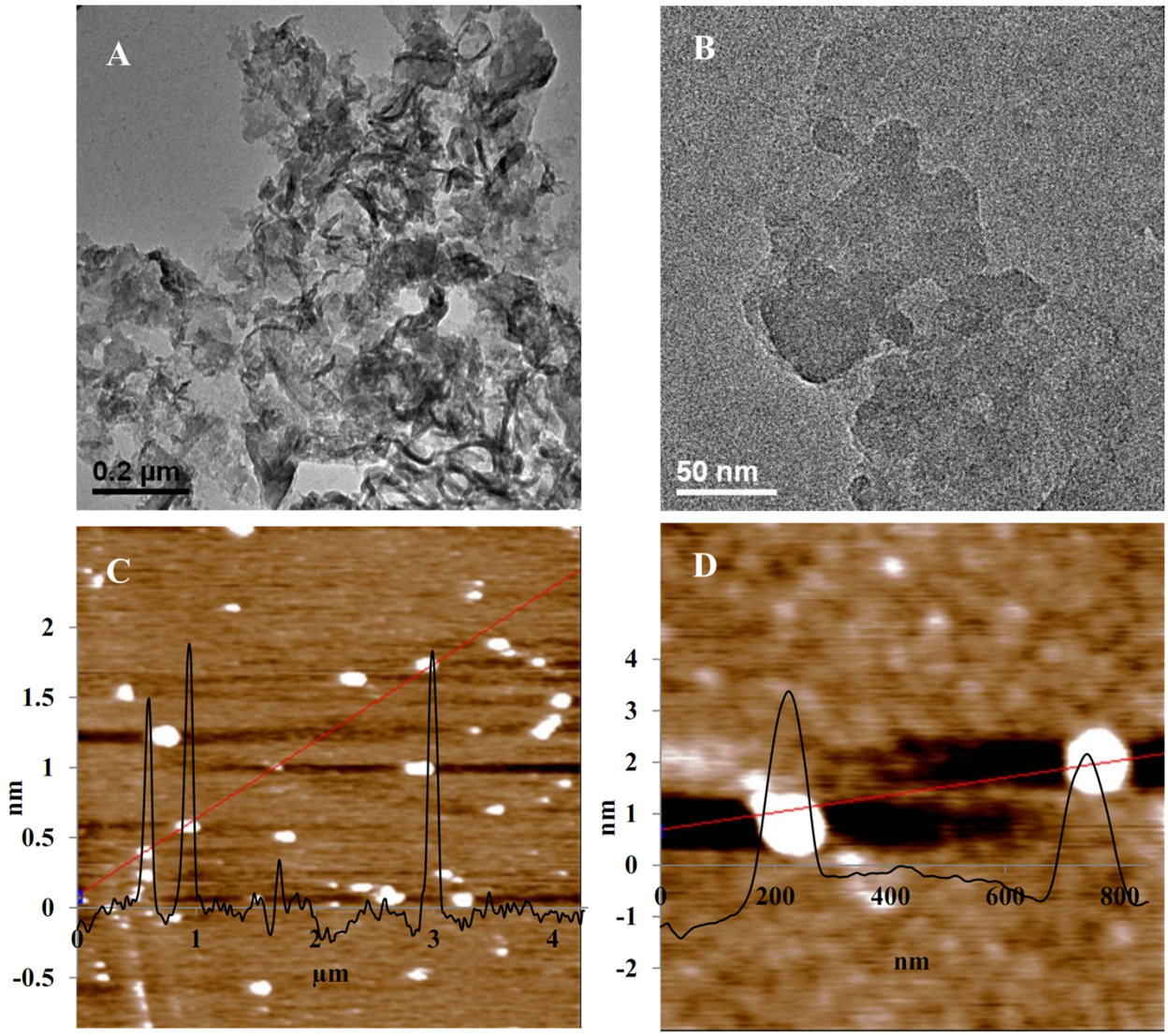

Figure S2. TEM images of CN (A) and CNs (B) and AFM images (C and D) of CNs. The insets in C and D are the height profile of CNs.

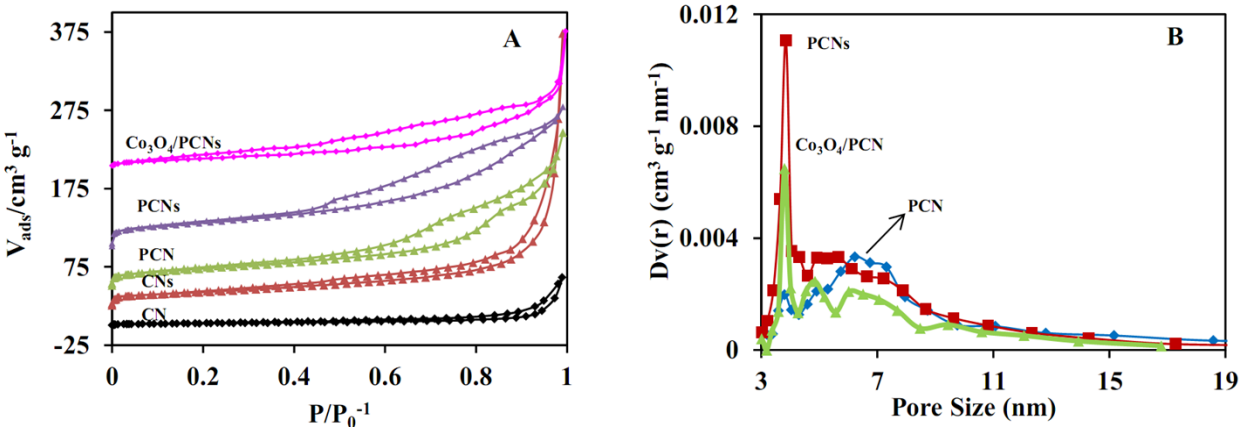

Figure S3. Adsorption isotherms (A) of CN, CNs, PCN, PCNs and 3.82%-Co_3O_4/PCNs. The isotherms are offset by 25, 50, 100 and 200 cm^3 g^{-1} for CNs, PCN, PCNs and 3.82%-Co_3O_4/PCNs, respectively; and BJH pore size distribution (B) of PCN, PCNs and 3.82%-Co_3O_4/PCNs.

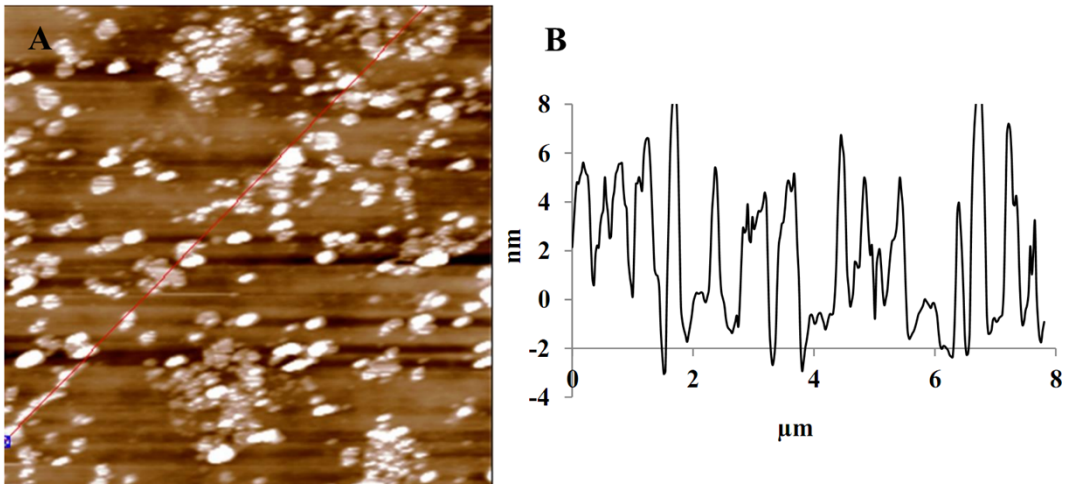

Figure S4. AFM image (A) and height profile (B) of 3.82%-Co_3O_4/PCNs.

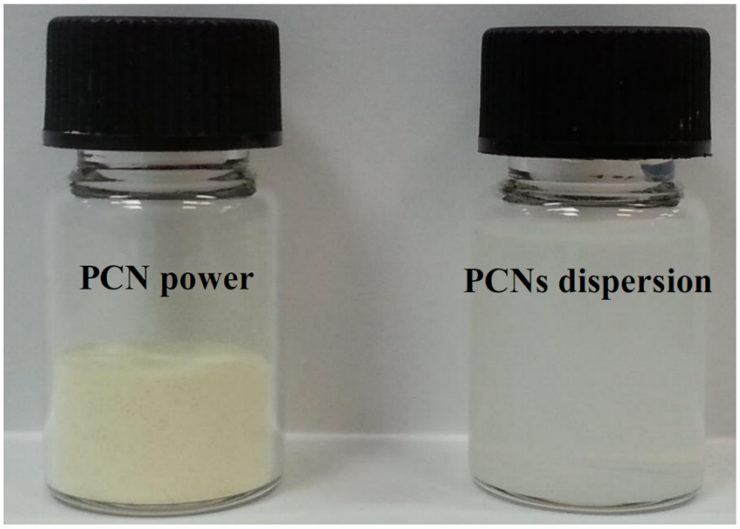

Figure S5. Photos of PCN powder and PCNs suspension in water.

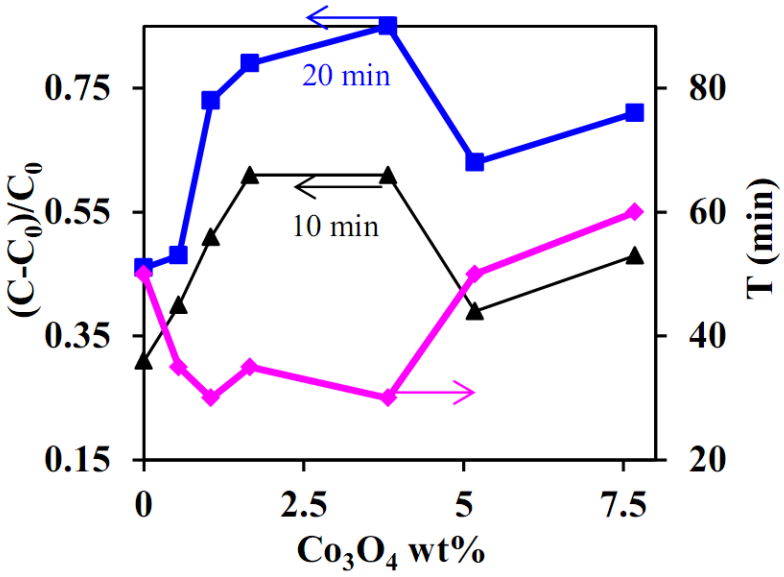

Figure S6. The effect of Co_3O_4 loading percentage on dye degradation performance. The degradation percentages of RhB at 10 min and 20 min, and the time needed for total degradation versus Co_3O_4% were plotted.

Figure S7. TEM images of Fe_3O_4/PCNs (A, B), NiO/PCNs (C, D) and CuO/PCNs (E, F). The lattice of Fe_3O_4 (JCPDS #88-0866), NiO (JCPDS #01-1239) and CuO (JCPDS #01-1117) are labelled in Figure S7B, D, F, respectively.

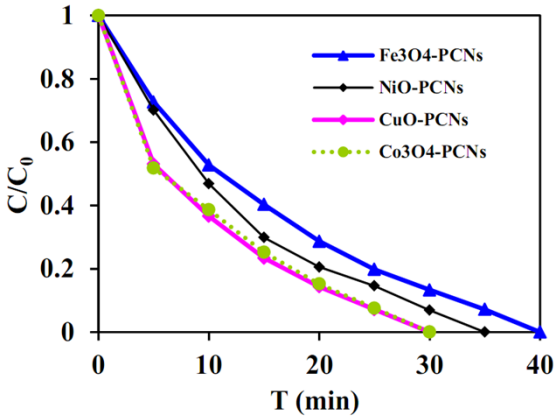

Figure S8. Photocatalytic degradation of RhB over different metal oxides (Fe_3O_4, NiO, CuO and Co_3O_4) loaded PCNs with around 4.0 wt% of metal oxides.

Macroporous C_3N_4 nanosheets

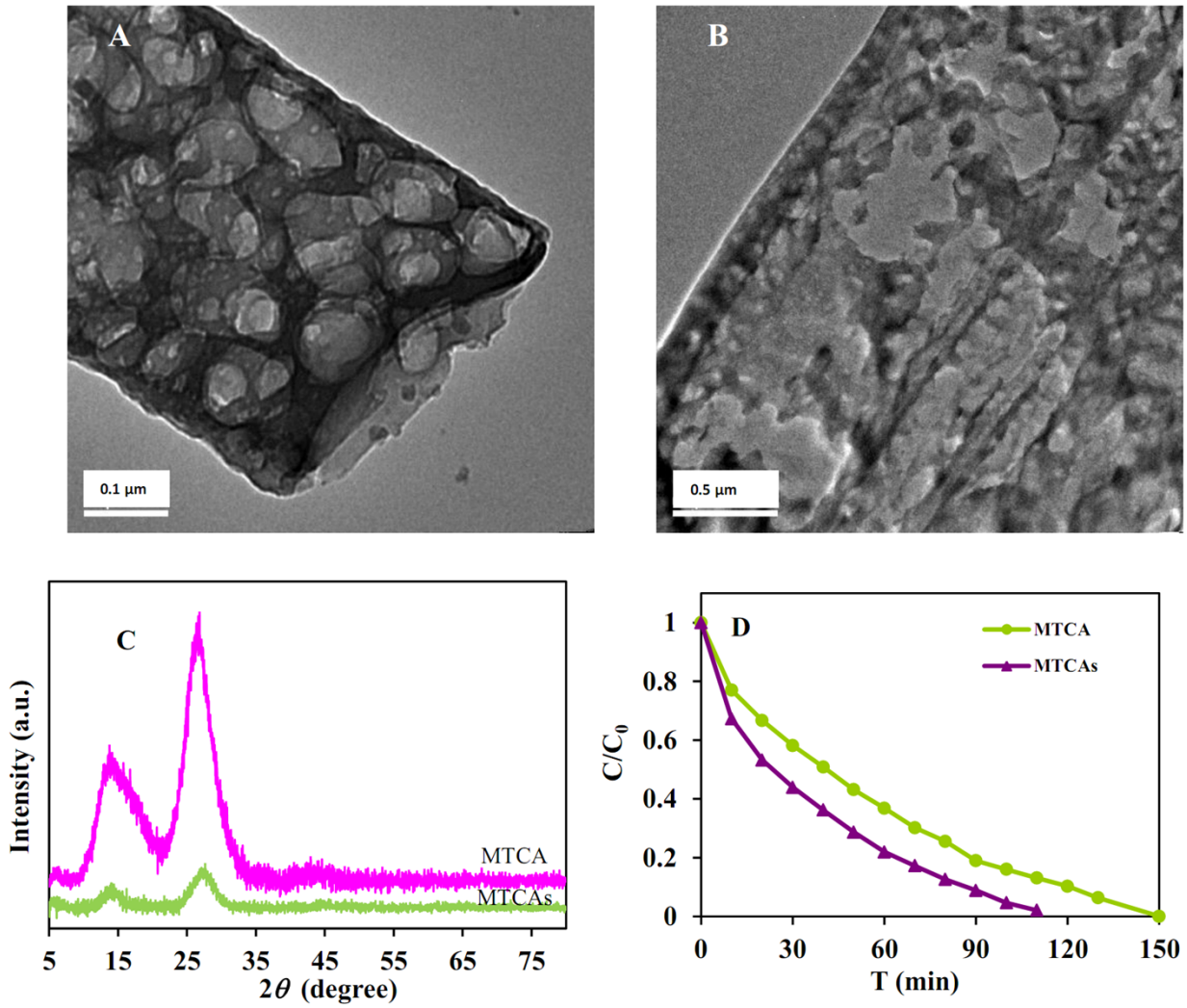

Figure S9. TEM images of MTCA (A) and MTCA nanosheets, MTCAs (B); XRD patterns (C) of MTCA and MTCAs; and (D) RhB degradation over MTCA and MTCAs. Reaction conditions: 5 mg of catalyst (without cocatalyst loading), 100 mL Rhodamine B (10 mg L^{-1}) with 0.01 M H_2O_2, 300 W Xe lamp without filter as the light source.

Macroporous C_3N_4 was prepared according to the literature.[1] Briefly, melamine (3.96 mmol) and trithiocyanuric acid (3.96 mmol) were dissolved in 20 mL of dimethyl sulfoxide (DMSO) at 30 °C, respectively. These two solutions were mixed under vigorous stirring. After stirring for 10 min, 30 mL of H_2O was added into the above mixture to form melamine-trithiocyanuric acid complex (MTCAc). The MTCAc was filtrated and washed thoroughly with deionized H_2O to remove DMSO. After dried at 90 °C in a vacuum oven overnight, the MTCAc was calcinated at 550 °C for 4 h under static air. The obtained dark yellow powder was named as MTCA.

To prepare MTCA nanosheets, 50 mg of MTCA sample was dispersed in 50 mL of different solvents (dimethyl sulfoxide, 1,4-dioxane, dimethylformamide, acetonitrile, acetone, ethanol,

ethanol, isopropanol and H_2O). MTCA can be dispersed best in 1,4-dioxane which was further undergoing probe ultrasonication for 2 h. The obtained suspension was centrifuged at 1,000 rpm for 1 min and the un-exfoliated MTCA at the bottom were removed. The top supernatant was centrifuged at 20,000 rpm for 5 min, dried at 60 °C and collected for characterization.

Figure S9A shows that the as-obtained MTCA has a three-dimensional porous structure with its macropores of around 100 nm. A similar observation was found in literature. MTCA nanosheets (MTCAs) obtained by exfoliation using probe sonication are much thinner as observed from the TEM image (Figure S9B). XRD patterns in Figure S9C showed that both the in-planar peak at 13° and interlayer-stacking at 27° are much weaker, indicating the reduction of the thickness of MTCA. Dye degradation study using RhB as the model dye in Figure S7D reveals that MTCAs has a higher activity than the un-exfoliated MTCA.

Table S1 Summary of photocatalytic data from pollutant degradation over carbon nitride based photocatalysts.

[mg] Photocatalyst	**[mg/L] Dye**	**V, mL**	**Light source**	**Time for complete degradation**	**Ref.**
[40] Fe/CN	[10] RhB[a]	80	500W, >420 nm	9 h	2
[300] CN	[0.4] MO[b]	100	300W, > 420 nm	5 h	3
[200] B doped CN	[4] MO [4] RhB	100	300W, > 420 nm	5 h 40 min	4
[100] S doped CN	[30] Phenol	100	300W, >420 nm	10 h	5
[150] Ag/CN	[10] MO	50	500W, >420 nm	3 h	6
[100] CN	[10] MB[c]	100	300W, > 400 nm	100 min	7
[5] CN [5] CNs	[10] RhB	100	300W, > 300 nm	180 min 60 min	8
[40] CN	[80] RhB [80] 4-CP[d] [80] Phenol	80	300W, > 420 nm	60 min 3 h 3 h	9
[45] Au/CNs [45] Au/CN	[10] MO	15	500W, > 400 nm	2.5 h 40% @ 2.5h	10
[25] CNs [25] CN	[20] MB	25	500W, > 420 nm	4 h 20% @ 4h	11
[5] CN	[10] RhB	5	LED 12W, >420 nm	105 s	12
[100] Co_3O_4/CN	[10] MO	100	250W, >420 nm	3 h	13
[5] Co_3O_4/CN [5] Co_3O_4/CNs [5] Co_3O_4/PCN [5] Co_3O_4/PCNs [5] PCNs	[10] RhB	100	300W	120 min 90 min 60 min 30 min 50 min	This work
[5] Co_3O_4/PCNs	[10] RhB	100	300W, > 420 nm	180 min	This work

[a] RhB: Rhodamine B; [b] MO: Methyl Orange; [c] MB: Methylene Blue; [d] 4-CP: 4-cholorphenol.

Effect of bath and probe sonication

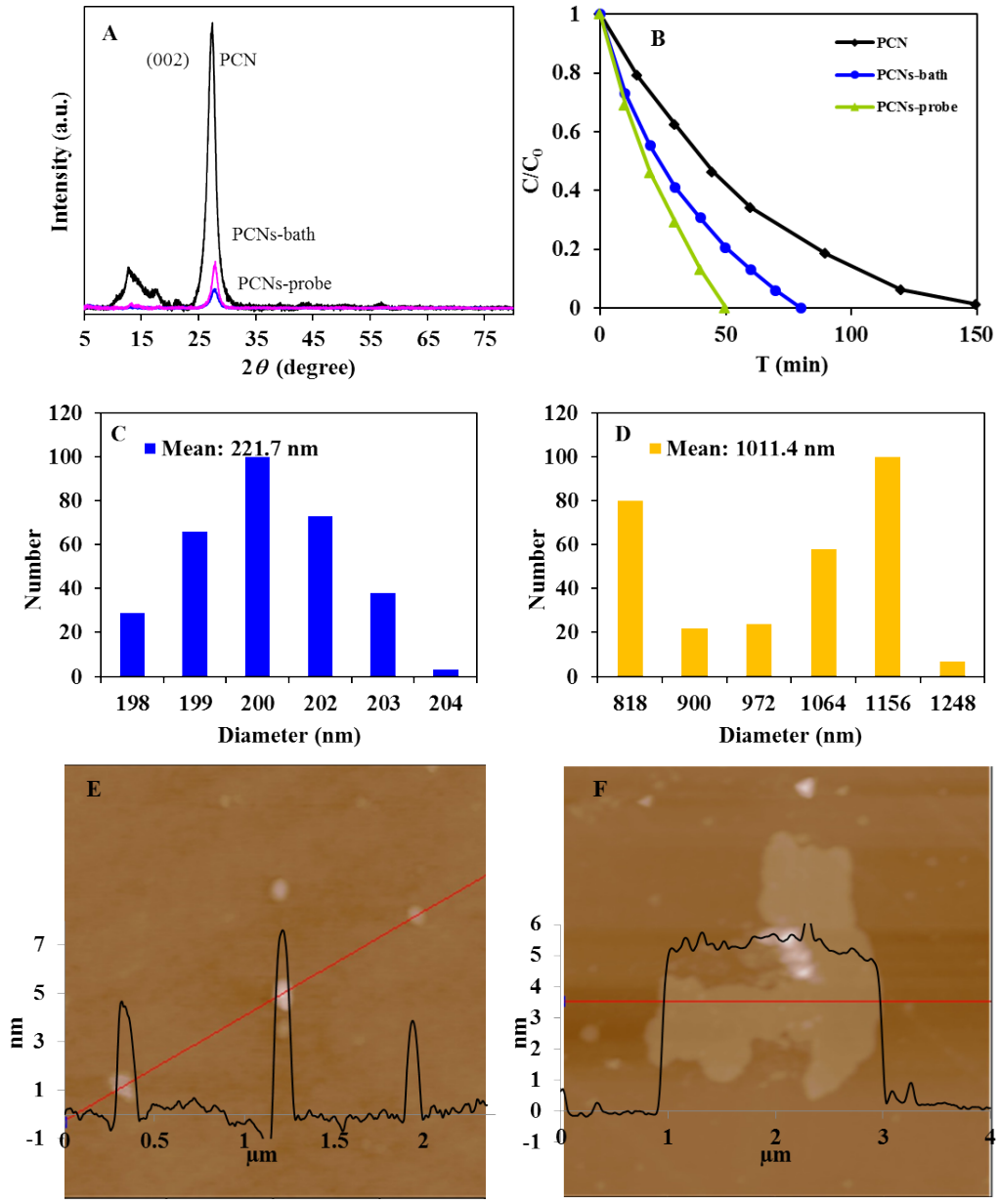

Figure S10. XRD patterns (A) of PCN and PCNs from bath (16 h) or probe sonication (2 h), and photocatalytic degradation of RhB (B) over PCN, PCNs from bath or probe sonication; the reaction conditions were the same as those for Figure 6. DLS Particle size distributions of PCNs from probe sonication (C) and bath sonication (D). AFM images of PCNs from probe sonication (E) and bath sonication (F).

It was found that most of the previous work reported in the literature adopted bath sonicator for liquid exfoliation of carbon nitride nanosheets. It is well-known that there is a distribution of ultrasonic energy within the liquid in the bath sonicator.[14, 15] Hence, the quality of different batches of carbon nitride nanosheets may not be consistent if the ultrasonic position is not fixed.

In addition, the bath sonicator has a relative weak energy intensity which requires longer time (generally more than 10 h) to obtain the nanosheets with thickness of several nm. However, there is not yet detailed discussion on the effect of the intensity distribution in a bath sonicator and its comparison with probe sonicator. The information of bath sonicator such as brand and power are usually not stated, though they are critical on the preparation of nanosheets. Here we conducted a comparison of these two kinds of ultrasonication for the preparation of PCNs.

For bath sonication, 50 mg of PCN was dispersed in 50 mL of ethanol and ultrasonicated for 16 h in a 300 W bath sonicator (Model: DC200H, Taiwan Delta New Instrument Co. ltd). For probe sonication, a 750 W Sonics Vibra-cell at 90% amplitude (model VCX 750, Sonics & Materials, Inc., USA) was applied for 2 h. The obtained suspension was centrifuged at 6,000 rpm for 5 mins and the top suspension was collected for characterization and used for degradation of RhB. Particle size distribution of the suspensions was obtained at room temperature using dynamic light scattering (DLS) technique on 90 Plus Particle Size Analyzer (Brookhaven Instruments Corporation).

Based on the XRD patterns in Figure S10, the PCNs from the probe exfoliation shows a weaker intensity than the PCNs from the batch sonicator, indicating a narrow stacking thickness of PCNs. With a strong power (750 W), a much shorter ultrasonication duration of 2 h using the probe sonicator can lead to a better or at least comparable exfoliation with 16 h ultrasonication using bath sonicator. Figure S10B shows that PCNs from the probe exfoliation can degrade RhB more efficiently, with around 30% less time needed for complete degradation of RhB.

Furthermore, DLS measurement results in Figure S10C and D show that PCNs from probe sonication has much smaller particle size distribution (with mean value of 221.7 nm) than that from bath sonication (with mean value of 1011.4 nm). Hence, probe sonicator with a stronger power (750W) causes the reduction in the lateral size while exfoliating carbon nitride layers. The obvious size difference can also be found in their AFM images in Figure S10E and F. As the nanosheets are not spherical, DLS measurement cannot tell the actual lateral size of the nanosheets. According to Colman's study on different nanosheets of graphene, MoS_2, WS_2, a fitting equation was derived for the correlation of DLS measurement with TEM determined size.[16] Generally, the size from DLS will be lower than that from TEM measurement considering a quasi-sphere model used for DLS measurement.

References:

1. Y. S. Jun, J. Park, S. U. Lee, A. Thomas, W. H. Hong and G. D. Stucky, *Angew. Chem. Int. Ed.*, 2013, **125**, 11289-11293.
2. X. C. Wang, X. F. Chen, A. Thomas, X. Z. Fu and M. Antonietti, *Adv. Mater.*, 2009, **21**, 1609-1612.
3. S. C. Yan, Z. S. Li and Z. G. Zou, *Langmuir*, 2009, **25**, 10397-10401.
4. S. C. Yan, Z. S. Li and Z. G. Zou, *Langmuir*, 2010, **26**, 3894-3901.
5. G. Liu, P. Niu, C. H. Sun, S. C. Smith, Z. G. Chen, G. Q. Lu and H.-M. Cheng, *J. Am. Chem. Soc.*, 2010, **132**, 11642-11648.
6. L. Ge, C. C. Han, J. Liu and Y. F. Li, *Appl. Catal. A: General*, 2011, **409**, 215-222.
7. J. H. Liu, T. K. Zhang, Z. C. Wang, G. Dawson and W. Chen, *J. Mater. Chem.*, 2011, **21**, 14398-14401.
8. X. D. Zhang, X. Xie, H. Wang, J. J. Zhang, B. C. Pan and Y. Xie, *J. Am. Chem. Soc.*, 2013, **135**, 18-21.

9. Y. J. Cui, Z. X. Ding, X. Z. Fu and X. C. Wang, *Angew Chem., Int. Ed.*, 2012, **124**, 11984-11988.
10. N. Y. Cheng, J. Q. Tian, Q. Liu, C. J. Ge, A. H. Qusti, A. M. Asiri, A. O. Al-Youbi and X. P. Sun, *ACS Appl. Mater. Interfaces*, 2013, **5**, 6815-6819.
11. J. Xu, L. W. Zhang, R. Shi and Y. F. Zhu, *J. Mater. Chem. A*, 2013, **1**, 14766-14772.
12. M. Shalom, S. Inal, C. Fettkenhauer, D. Neher and M. Antonietti, *J. Am. Chem. Soc.*, 2013, **135**, 7118-7121.
13. C. C. Han, L. Ge, C. F. Chen, Y. J. Li, X. L. Xiao, Y. N. Zhang and L. L. Guo, *Appl. Catal. B: Environ.*, 2014, **147**, 546-553.
14. J. K. Jiang, G. Oberdörster and P. Biswas, *J. Nanopart. Res.*, 2009, **11**, 77-89.
15. J.-L. Capelo-Martínez, *Ultrasound in chemistry: analytical applications*, John Wiley & Sons, 2008.
16. M. Lotya, A. Rakovich, J. F. Donegan and J. N. Coleman, *Nanotechnology*, 2013, **24**, 265703.